Efflorescence Relative Humidity for Ammonium Sulfate Particles

Yonggang Gao, Shing Bor Chen,* and Liya E. Yu†

Department of Chemical and Biomolecular Engineering, National University of Singapore, Singapore 117576

Received: December 30, 2005; In Final Form: March 15, 2006

The classical homogeneous nucleation theory was employed to calculate the efflorescence relative humidity (ERH) of airborne ammonium sulfate particles with a wide size range (8 nm to 17 μm) at room temperature. The theoretical predictions are in good agreement with the experimentally measured values. When the ammonium sulfate particle is decreased in size, the ERH first decreases, reaches a minimum around 30% for particle diameter equal to about 30 nm, and then increases. It is for the first time that the Kelvin effect is theoretically verified to substantially affect the ERH of ammonium sulfate particles smaller than 30 nm, while the aerosol size is the dominant factor affecting the efflorescent behavior of ammonium sulfate particles larger than 50 nm.

1. Introduction

Airborne particles from various sources, such as sea spray, volcano eruption, and anthropogenic emission can influence the radiation balance of earth and cloud formation.[1−4] The amount of water in a particle depends on the atmospheric relative humidity (RH) and the water sorption property of airborne particles. Certain atmospheric particles can undergo water uptake at sufficiently high RH (deliquescent process) and substantially grow in size, which can alter their light scattering behavior and/or chemical reactions in the atmosphere. Upon decreasing RH, a hysteresis behavior can be observed when wet particles decrease in size through losing water to eventually crystallize (efflorescent process). Ammonium sulfate (AS) aerosol is one of the major inorganic species in atmosphere.[5−7] Its deliquescent and efflorescent behaviors have been studied using various experimental techniques, which are summarized in Table 1. While similar values for deliquescence relative humidity (DRH), ranging between 79% and 81%, were obtained by various research groups, the reported efflorescence relative humidity (ERH) varies substantially (33−48%) (Table 1).

Unlike DRH that can be described by thermodynamic principles, ERH is mainly governed by kinetics of homogeneous or heterogeneous nucleation.[1,4] While the homogeneous nucleation demands a high degree of supersaturation, the heterogeneous nucleation can be catalyzed by existing foreign solids in a less supersaturated solution.[13] For the cases of homogeneous nucleation, Onasch et al.[14] determined the critical nucleation rate from $J_c = 1/(V_e t)$, where t is the induction time and V_e is the particle volume at efflorescence. They then applied the Gibbs−Duhem relation, the thermodynamic model of Clegg et al.,[15,16] and the experimentally obtained DRH and ERH to calculate the critical supersaturation S^*. On the basis of classical nucleation theory, the energy barrier, which can be calculated from the critical nucleation rate, depends both on the supersaturation and on the droplet interfacial tension. Accordingly, a plot of J_c vs $(\ln S^*)^{-2}$ should be a straight line, provided that the temperature and interfacial tension are both constant. For most experimental data, this behavior is observed, and the interfacial tension that is determined from the fitting line slope falls in the middle of the range reported in the literature. Despite the application of nucleation theory, this work did not directly predict ERH and growth factor prior to efflorescence.

TABLE 1: DRH and ERH Reported in Literatures

particle size	DRH	ERH	technique	ref
<50 nm	79−81%		TDMA	6
100 nm	79 ± 1%		TDMA[b]	8
300 nm	80%	35%	FTIR	9
450[a]nm	79 ± 1%	33 ± 1%	FTIR[c]	10
1 μm	80%	35%	FTIR	11
20[a]μm	81%	48%	EDB[d]	12

[a] Initial droplet particle size. [b] Tandem differential mobility analyzer system. [c] Fourier transform infrared spectrometer. [d] Electrodynamic balance.

While several theoretical works for calculation of DRH of aerosols have been reported,[17−19] a direct prediction of ERH of an aerosol particle with a given size is not yet available in the literature. Hence, the present work aims to utilize the well-established classical nucleation theory as the framework to calculate the growth factor and determine the ERH of AS particles of a wide size range, spanning from 8 nm to 17 μm. For the first time, the Kelvin effect is theoretically verified to be most influential on particles smaller than 30 nm, in agreement with the recent experimental observation on sodium chloride particles.[20] The theoretical predictions are compared with the experimental data measured in this work and reported in the literature.

2. Basic Theories and ERH Prediction

2.1. The Kelvin Effect on Relative Humidity (Köhler Equation). The relative humidity RH $= p/p_w$ is defined as the ratio of the actual water vapor pressure (p) in the air to the saturation value (p_w) at a specific temperature. For an ideal aqueous solution, the water vapor pressure follows the Raoult's law: $p_{sol} = x_w p_w$, where x_w is the mole fraction of water in the solution, and thus RH $= x_w$. For a nonideal solution, however, the Raoult's law is modified to be

$$\frac{p_{sol}}{p_w} = \gamma_w x_w = a_w = \mathrm{RH} \qquad (1)$$

* To whom correspondence should be addressed. E-mail: checsb@nus.edu.sg.
† Division of Environmental Science & Engineering, NUS, Singapore.

10.1021/jp057574g CCC: $33.50
Published on Web 05/25/2006

where a_w and γ_w represent the activity and the activity coefficient of water, respectively. Equation 1 is valid for a bulk aqueous solution. For a nanometric aqueous droplet, the Kelvin effect accounts for an increase in the equilibrium vapor pressure (p_c) due to the air−liquid interface curvature, compared with the corresponding value (p_{sol}) for a flat surface. This Kelvin equation can be expressed as

$$I_{kelvin} = \frac{p_c}{p_{sol}} = \exp\left(\frac{4M_w\gamma_{drop-air}}{RT\rho_w D}\right) \quad (2)$$

where D is the droplet diameter, M_w and ρ_w are the molar mass and density of water, R is the molar gas constant (8.314 $J\cdot mol^{-1}\cdot K^{-1}$), T is absolute temperature, and $\gamma_{drop-air}$ is the surface tension at the droplet interface. When calculating RH surrounding an aqueous droplet, the Kelvin effect should be incorporated into eq 1, thereby leading to the Köhler equation

$$RH = \frac{p_c}{p_w} = \gamma_w x_w I_{kelvin} = a_w \exp\left(\frac{4M_w\gamma_{drop-air}}{RT\rho_w D}\right) \quad (3)$$

2.2. Homogeneous Nucleation in an Aqueous Droplet. We apply homogeneous nucleation theory to investigate the efflorescence of an electrolyte droplet. When the RH is approaching the ERH of an electrolyte droplet, the droplet is becoming increasingly supersaturated. The free energies of the supersaturated droplet prior to nucleation (state 1) and at the ERH when the first nucleus forms (state 2) are, respectively, given by

$$G_1 = \mu_1 N + \gamma_{drop-air}A_{drop-air} \quad (4)$$

$$G_2 = \mu_2 i + \mu_1(N-i) + \gamma_{drop-air}A_{drop-air} + \gamma_{drop-nuc}A_{drop-nuc} \quad (5)$$

μ_1 is the solute chemical potential in the supersaturated solution, μ_2 is the solute chemical potential in the nucleus, i is the molecule number of the solute in the nucleus, γ is the interfacial tension, and A represents the interfacial area. The change in Gibbs energy (ΔG) from state 1 to state 2 represents the work required for the inception of crystal embryos from the solution and is given by

$$\Delta G = G_2 - G_1 = -(\mu_1 - \mu_2)\cdot i + \gamma_{drop-nuc}A_{drop-nuc} \quad (6)$$

To arrive at the above equation, we have neglected the change in $A_{drop-air}$ from state 1 to 2. This assumption will be justified later.

Since the solute chemical potential in the crystal must equal the value in the saturated solution, namely, $\mu_2 = \mu_1^0$, the chemical potential difference for super saturation is $\Delta\mu = \mu_1 - \mu_1^0$. Assuming the shape of the solute crystal to be spherical, eq 6 becomes

$$\Delta G = -\Delta\mu\frac{4\pi r^3}{3\nu_c} + \gamma_{drop-nuc}4\pi r^2 \quad (7)$$

where ν_c is the volume of a solute molecule and r is the radius of the nucleus. The first term on the right-hand side represents the chemical work, which is negative reflecting the supersaturated solution; the second term is the mechanical work required for the formation of the embryo. In eq 7, the difference in chemical potential can be expressed as $\Delta\mu = K_B T \ln S$ with $S = a/a_0$ being the supersaturation ratio, where a is the solute activity in the supersaturated solution, a_0 is the solute activity of the saturated solution, and K_B is the Boltzmann constant.

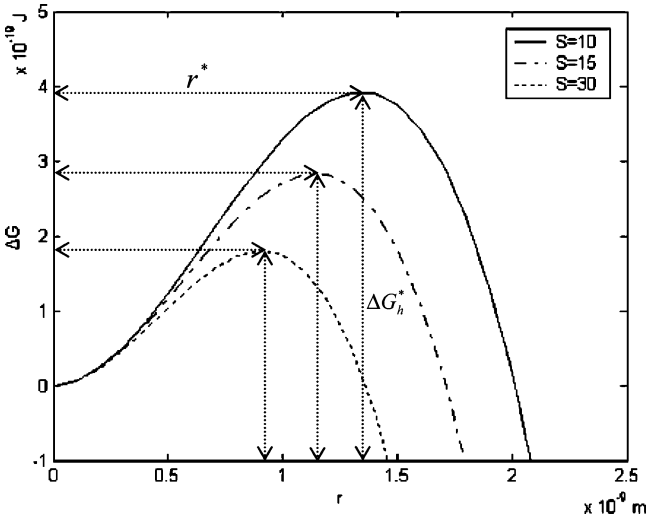

Figure 1. Variation of the Gibbs energy change for nucleation at three different values of supersaturation (S). ΔG_h^* is the barrier energy, and r^* is the corresponding critical radius.

According to the nucleation theory, the energy barrier is the maximum ΔG that can be determined by

$$\frac{d\Delta G}{dr} = -\frac{4\pi r^2}{\nu_c}K_B T \ln S + \gamma_{drop-nuc}8\pi r = 0$$

Solving the above equation finds the critical radius of the nucleus

$$r^* = \frac{2\gamma_{drop-nuc}\nu_c}{K_B T \ln S} \quad (8)$$

Substituting eq 8 to eq 7 yields the energy barrier

$$\Delta G_h^* = \frac{16\pi\gamma_{drop-nuc}^3\nu_c^2}{3(K_B T \ln S)^2} \quad (9)$$

which is also called nucleation work. Figure 1 illustrates the change in the Gibbs energy with the nucleus radius for airborne AS particles at room temperature using eq 7 with $\nu_c = 1.24 \times 10^{-28}$ m^3 and $\gamma_{drop-nuc} = 0.052$ N/m.[14]

2.3. Homogeneous Nucleation Rate. For homogeneous nucleation, the formation rate for a unit volume of a critical nucleus in a supersaturated droplet is expressed as

$$J = J_0 e^{-\Delta G_h^*/K_B T} \quad (10)$$

where the kinetic factor J_0 is a measure of the attempt frequency for a molecule in the liquid to become involved in the critical nucleus and has been found to be about 10^{38} m^{-3} s^{-1}.[13,14,21] This rate at the efflorescence point can be estimated by[13,14,22]

$$J_c = \frac{1}{V_e t} \quad (11)$$

where V_e is the volume of the supersaturated droplet at this point and t is the nucleation induction time, which is the time interval between the establishment of supersaturation and the formation of critical nuclei.

2.4. Prediction of ERH for Ammonium Sulfate Droplets. The independent variable for the ERH calculation in the present study is the dry particle diameter (D_{dry}). Given a specified D_{dry}, we vary the salt molality m in the droplet, and the corresponding

TABLE 2: Calculated Quantities as Functions of Molality at 298 K for an AS Particle with a Dry Diameter of 100 nm

m (mol/kg)	GF	D (nm)	RH (×100%)	S	G^*_h (J)	J (m^{-3} s^{-1})	r^* (m)
2	1.964	196.4	92.5				
4	1.624	162.4	85.0				
5.8[a]	1.483	148.3	78.6	1			
6	1.474	147.4	78.0	1.07	4.532×10^{-16}	0	4.56×10^{-8}
8	1.388	138.8	71.7	2.13	3.653×10^{-18}	0	4.10×10^{-9}
10	1.331	133.1	66.1	3.57	1.282×10^{-18}	3.97×10^{-96}	2.43×10^{-9}
12	1.290	129.0	61.0	5.39	7.328×10^{-19}	5.71×10^{-39}	1.83×10^{-9}
16	1.236	123.6	52.5	9.97	3.933×10^{-19}	1.20×10^{-3}	1.34×10^{-9}
18	1.218	121.8	48.9	12.63	3.234×10^{-19}	2.27×10^{4}	1.22×10^{-9}
20	1.202	120.2	45.6	15.46	2.773×10^{-19}	1.42×10^{-9}	1.13×10^{-9}
22	1.189	118.9	42.8	18.43	2.449×10^{-19}	3.32×10^{12}	1.06×10^{-9}
26	1.169	116.9	37.8	24.58	2.028×10^{-19}	7.93×10^{16}	9.65×10^{-10}
28	1.161	116.1	35.7	27.70	1.885×10^{-19}	2.45×10^{18}	9.30×10^{-10}
30	1.154	115.4	33.8	30.80	1.770×10^{-19}	3.87×10^{19}	9.01×10^{-10}
33.3[b]	1.144	114.4	31.0	35.81	1.624×10^{-19}	1.27×10^{21}	8.63×10^{-10}
36	1.137	113.7	29.0	39.91	1.530×10^{-19}	1.21×10^{22}	8.38×10^{-10}
38	1.132	113.2	27.7	42.83	1.473×10^{-19}	4.74×10^{22}	8.22×10^{-10}
40	1.128	112.8	26.5	45.67	1.424×10^{-19}	1.54×10^{23}	8.08×10^{-10}
42	1.124	112.4	25.4	48.44	1.381×10^{-19}	4.30×10^{23}	7.96×10^{-10}
44	1.121	112.1	24.3	51.14	1.343×10^{-19}	1.06×10^{24}	7.85×10^{-10}
46	1.118	111.8	23.4	53.75	1.310×10^{-19}	2.36×10^{24}	7.75×10^{-10}
48	1.115	111.5	22.5	56.28	1.280×10^{-19}	4.82×10^{24}	7.67×10^{-10}
50	1.112	111.2	21.6	58.74	1.253×10^{-19}	9.14×10^{24}	7.59×10^{-10}
52[c]	1.110	111.0	20.9	61.11	1.229×10^{-19}	1.63×10^{25}	7.51×10^{-10}

[a] Molality of solution at saturation.[24,27] [b] Molality of solution at efflorescence point. [c] Initial value for iterative calculation.

salt mass fraction w can be determined by

$$w = \frac{M_{salt} m}{1000 + M_{salt} m} \tag{12}$$

where M_{salt} is molar mass (132 g/mol for AS). The density and surface tension of the droplet are calculated using the fitting equations (in SI units) of Tang and Munkelwitz[23] and Korhonen et al.,[24] respectively

$$\rho_{sol} = (0.9971 + 5.92 \times 10^{-1} \times w - 5.036 \times 10^{-2} \times w^2 + 1.024 \times 10^{-2} \times w^3) \times 1000 \tag{13}$$

$$\gamma_{drop-air} = 0.07191213 + 0.02238717 \times w - 0.07996065 \times w^2 + 0.69851611 \times w^3 - 2.36147549 \times w^4 + 4.29166949 \times w^5 - 3.66435817 \times w^6 + 1.14383687 \times w^7 \tag{14}$$

The droplet diameter (D) can be determined from the corresponding growth factor given by[25]

$$\mathrm{GF} = \frac{D}{D_{dry}} = \left\{ \frac{\rho_{salt}}{\rho_{sol}} [1 + (m M_{salt})^{-1}] \right\}^{1/3} \tag{15}$$

ρ_{salt} is the density of bulk salt, which is equal to 1769 kg/m^3 for AS.[8]

To proceed with the calculation of RH, ΔG^*_h, r^*, and J using eqs 3, 9, 8, and 10, it is necessary to determine the AS and water activities. Most of the reported empirical equations for the activities are valid for the AS molality up to about 28 mol/kg,[15,23,24,26−28] which unfortunately are inappropriate for this study, because the molality of a highly supersaturated droplet near ERH can be greater than 35 mol/kg. In view of this, we find suitable the work of Ally et al.,[29] which used statistical mechanics of multilayer adsorption based on the Brunauer−Emmett−Teller (BET) adsorption isotherm. Their predictions for water and salt activities in supersaturated aqueous solutions agree well with experimental data, even for highly supersaturated solutions (m > 35 mol/kg). In their model, the salt and water activities are given by

$$a_{salt} = [(qB - X)/qB]^q \tag{16}$$

$$a_w = (W - X)/W \tag{17}$$

where B and W represent the salt and water moles in the solution, respectively, and X is the amount of adsorbed water satisfying

$$X^2/[(qB - X)(W - X)] = \exp(-\epsilon_A/k_B T) = c_A \tag{18}$$

where q is the number of adsorption sites per mole of the salt and ϵ_A is the internal energy for a monolayer of water adsorbed onto the salt. The positive solution to the quadratic eq 18 gives the physically correct X value. For the $[(NH_4)_2SO_4 + H_2O]$ system, Ally et al.[29] reported $c_A = 2.075 \pm 0.293$ and $q = 2.47 \pm 0.476$.

In Table 2, we list the calculated quantities as functions of molality for AS particles with $D_{dry} = 100$ nm. Note that the molality of a saturated AS solution is 5.834 mol/kg at 298.15 K.[24,27] The way we determine the ERH is to ensure an identical nucleation rate calculated from both eqs 10 and 11 at a given induction time. Namely, we need to identify the value of m, at which such agreement can be achieved, since various physical quantities shown in Table 2 are functions of m. This can easily be accomplished by an iterative process as follows. Knowing the experimental observation[3,23,26,30] that GF is quite close to unity when efflorescence occurs, we use GF = 1.11 as an initial guess to facilitate the iterative calculation in order to find out the correct m and thus GF. At the given GF, the corresponding droplet volume is used to estimate the nucleation rate (J_c) from eq 11, which may not agree with the calculated J from eq 10. To correct GF, we compare the estimated J_c with the values of J listed in Table 2 and interpolate it to find the corresponding m, and hence obtain a new GF accordingly. These values will be used to determine a new V_e and thus J_c from eq 11 and J from eq 10. Such iteration is continued until the molality and growth factor converge to their final, correct values to result in identical J_c and J within tolerance. Note that the uniqueness of ERH calculated by this means has been verified by using

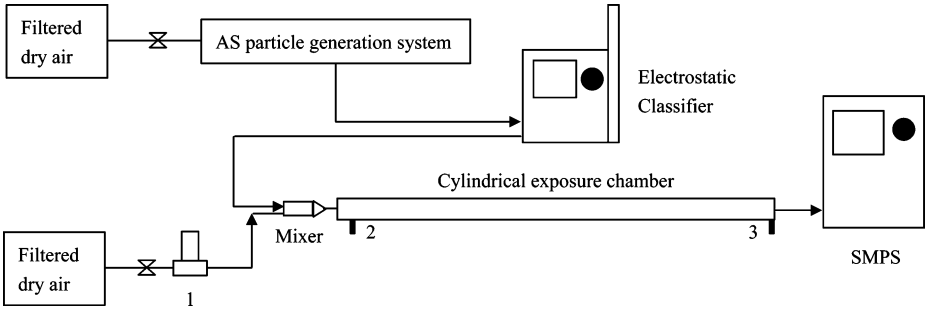

Figure 2. Schematic setup for ERH measurements of AS particles: (1) mass flow controller; (2,3) RH measurement ports.

different initial values of GF. For an AS particle with D_{dry} = 100 nm and induction time of 1 s, the ERH is predicted to be 31% (see Table 2), indicating that, under an RH < 31%, the AS particle is expected to be a dry solid with GF equal to unity. Table 2 also shows that G_n^* and r^* decrease, while J increases with the decreasing RH, implying a stronger tendency for the electrolyte droplet to undergo crystallization at lower RH, for which a higher degree of supersaturation results.

3. Experimental Section

To investigate the size change in the suspended AS particles under decreasing RH, a tandem differential mobility analyzer (TDMA) system was employed as Figure 2 shows, which consists of an electrostatic classifier (model 3080L; TSI, Inc., U.S.A.), an exposure chamber, and a scanning mobility particle sizer (model 3034 SMPS; TSI, Inc., U.S.A.). AS particles were produced through the atomization of a solution containing 0.2 wt % of $(NH_4)_2SO_4$ (purity > 99%, Merck, Germany). They were carried by air through the aerosol generation system followed by the particle size classifier with an aerosol-to-sheath flow rate of 0.1. The resulting monodispersed wet AS particles with a size around 80 nm at a flow rate of 1 ± 0.1 lpm were then mixed with a dry air stream (RH < 5%) prior to entering a cylindrical exposure chamber with length of 85 cm and inner diameter of 6 cm. A mass flow controller was utilized to provide the dry air stream at a flow rate between 0 and 2.5 lpm to vary the RH in the chamber and the residence time of the AS particles from 41 to 144 s. The final size of the airborne AS particles was monitored at the outlet of the tube reactor using the SMPS. Since the Reynolds number ranged from 23 to 80 (≪2100), the flow in the exposure chamber is laminar. It is known that the mixing effect in a laminar flow is not as good and may thus bring about nonuniform RH in the chamber. However, the size distribution of the examined particles was found to remain monomodal before (>70% RH) and after (<20% RH) drying conditions with a standard deviation of around ±10 nm, indicative of no serious problem of nonuniform RH and consequent efflorescence of a portion of particles.

The RH in the exposure chamber was adjusted spanning from 17% to 68% (Figure 3), which was monitored throughout the whole experiment using a thermohygrometer with a measurement precision of ±3% RH (Cole-Parmer, U.S.A.). In addition to a constant temperature (24.8 ± 0.3 °C) throughout the experiment, our prolonged in situ monitoring showed that the RH measured at the inlet and outlet of the exposure chamber (Figure 2) differed by less than 0.7% RH, demonstrating that the airborne AS particles were exposed to stable and consistent environment through the tube reactor.

The uncertainty of our experimental system was contributed by two factors: (1) the precision of the hygrometer (±3% RH); (2) the deviation of RH in the exposure chamber under a given flow condition. For the latter, on the basis of 14 sets of triplicate experiments, we found the deviation to be no larger than 3.8% RH. Hence, the propagated error throughout the whole experiment ranged from 5.2% to 6.4% RH. To verify the potential bias imposed by SMPS, we employed an established model[6] to estimate the RH in SMPS corresponding to the resultant growth factor of airborne ultrafine ammonium sulfate particles. Since the difference between the estimated RH in SMPS and that measured at the outlet of our exposure chamber ranged from 0.8% to 2.6% RH, the total propagated experimental error suffices to represent the overall experimental uncertainty.

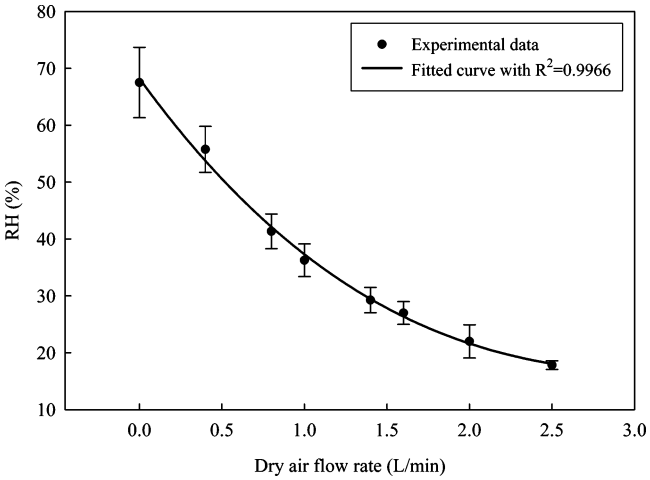

Figure 3. Effects of the flow rate of dry air on RH in the exposure tube.

4. Results and Discussion

Figure 4 shows that the experimentally obtained GF values of four nanometer-sized AS particles (8−50 nm) as a function of RH[6] satisfactorily agree with our theoretical estimation using the induction time of 0.15 s, which is indeed the estimated residence time from the same reference. Our theoretical estimation demonstrates the ERH for the AS particles ranging from 28% to 30% (Figure 4); the smallest (8 nm) AS particle appeared to have the highest ERH. The theoretically estimated ERH cannot be verified by the experimental data because the lowest RH (around 33%) provided in the previously conducted experiments[6] was too high to observe the actual ERH (Figure 4). Nevertheless, our experimental observation for a wide range of RHs found that the ERH for 43 and 47 nm AS particles is around 31%, acceptably consistent with the corresponding theoretical estimation as shown in Figure 5. Note that we have used the residence time of 60 s corresponding to the flow rate for the occurrence of efflorescence to conduct the theoretical calculations.

As mentioned in section 2, we have ignored the change in $A_{drop-air}$ from state 1 to 2 in the formulation of free energy

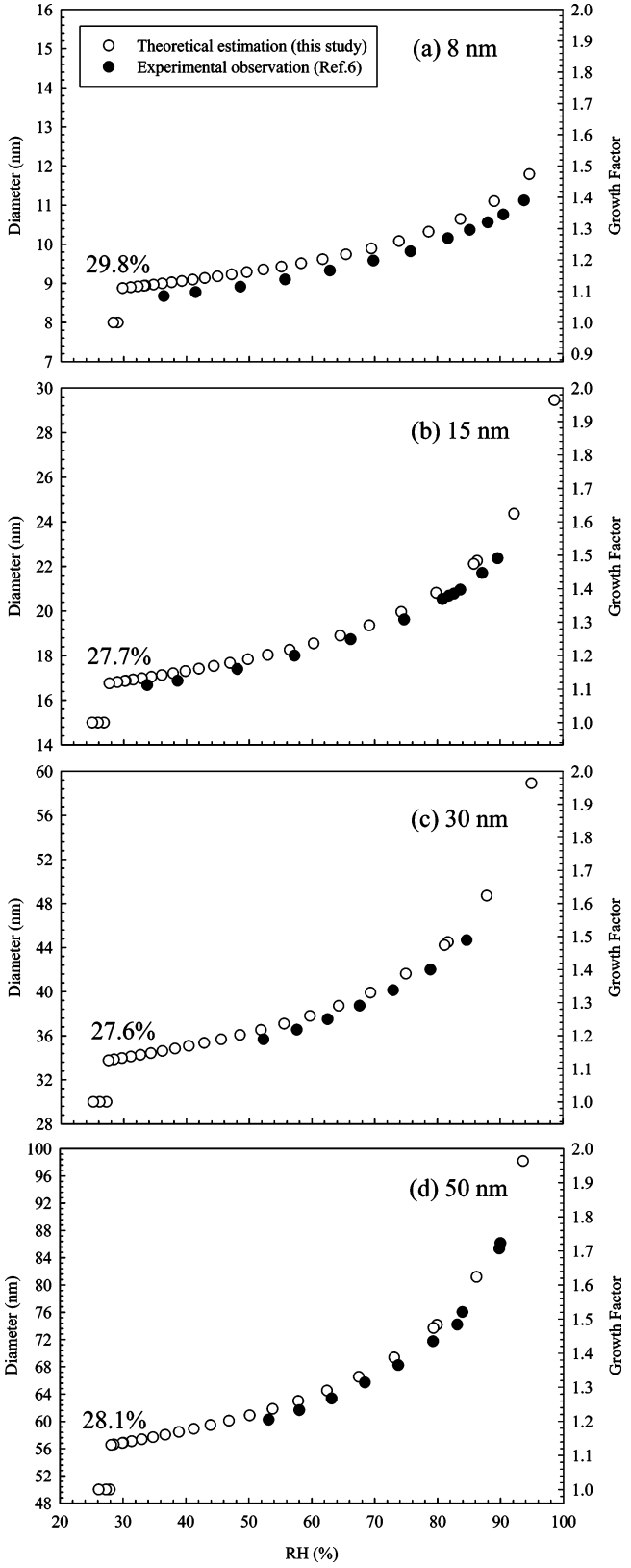

Figure 4. Growth factor and efflorescence trends for AS particles with dry-state diameters of (a) 8 nm, (b) 15 nm, (c) 30 nm, and (d) 50 nm.

difference. To examine this assumption, we calculate $\Delta A_{\text{drop-air}} = A_{\text{drop-air}}(2) - A_{\text{drop-air}}(1)$, which is negative, and determine $|\Delta A_{\text{drop-air}}|/A_{\text{drop-nuc}}$. This ratio is found to be very small, for example, equal to 0.003 for the case of dry particles of 8 nm. Since $\gamma_{\text{drop-air}}$ is comparable to $\gamma_{\text{drop-nuc}}$, the neglect of $\Delta A_{\text{drop-air}}$ is justifiable.

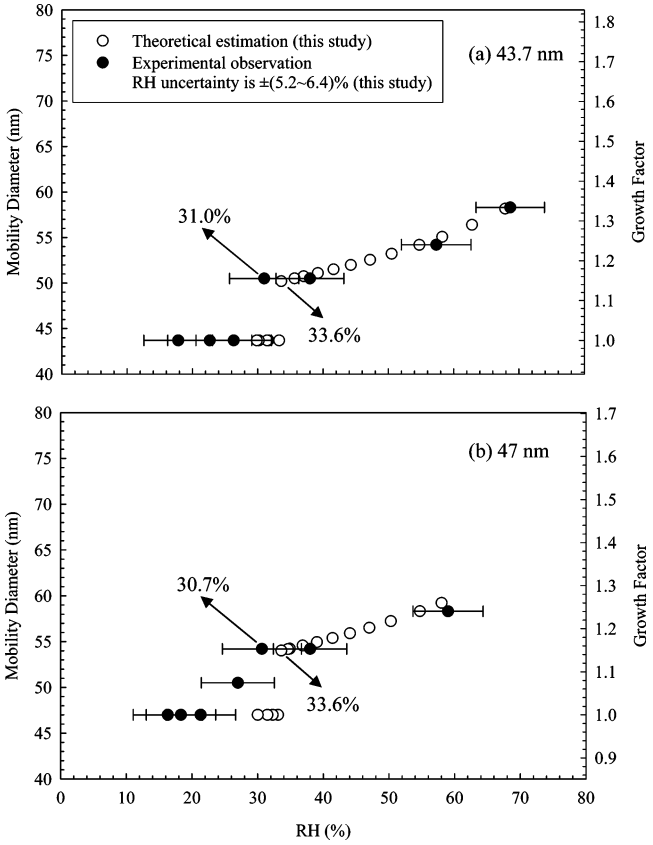

Figure 5. Growth factor and efflorescence trends for AS particles with dry-state diameters of (a) 43.7 nm and (b) 47 nm.

TABLE 3: Experimentally Obtained and Theoretically Calculated ERH

dry diameter (μm)	experimental ERH (%)	observation time(s)	calculated ERH (%)	ref
17[a]	47.48	1200[b]	42.7	26
10	37 ± 1.4%	1[b]	39.1	14
6−8	37−40	1[b]	38.2−38.7	23
5	37	1[b]	37.9	3
1	32.5	1[b]	35.3	31
1	35	30[c]	37.3	11
0.3	35	30[c]	35.6	9
0.28[a]	33 ± 2%	30[d]	35.6	10
0.03−0.08	38 and 40	1[b]	29.7−31	32
0.043 and 0.047	31 ± 6.4%	60[c]	33.6	this study

[a] Estimated on the basis of the reported initial diameter of droplet and growth factor. [b] Cited from ref 14. [c] Estimated on the basis of the residence time of particles in a reaction tube. [d] Reported in the ref.

In addition to predicting the ERH of AS particles in nanometer size, the theory employed in this study also effectively predicts the ERH of AS particles in micron size. For dry AS particles of 5 and 6 μm, Figure 6 shows a consistent trend between the published experimental data using electrodynamic balance (EDB) at the observation time of 1s[3,23] and the theoretical prediction in this study, with agreeable ERH between 37% and 38%. Hence, according to both experimental and theoretical results (Figures 4−6), the micron-sized particles appear to exhibit a higher ERH.

To further validate our theoretical prediction, Table 3 summarizes the experimentally obtained ERH of AS particles with sizes ranging from 30 nm to 17 μm in comparison with the theoretical prediction obtained in this study. The predicted ERHs show good agreement with the experimental data, except for the 0.03−0.08 μm AS particles. This could be due to the

TABLE 4: Calculated ERHs for AS Particles with Different Diameters[a]

D_{dry} (μm)	0.008	0.015	0.03	0.04	0.05	0.07	0.09	0.1	1	5	8	10	30
ERH (%)	33.0	30.3	29.7	29.8	30.0	30.5	30.9	31.0	35.3	37.9	38.7	39.1	40.5

[a] Induction time = 1 s.

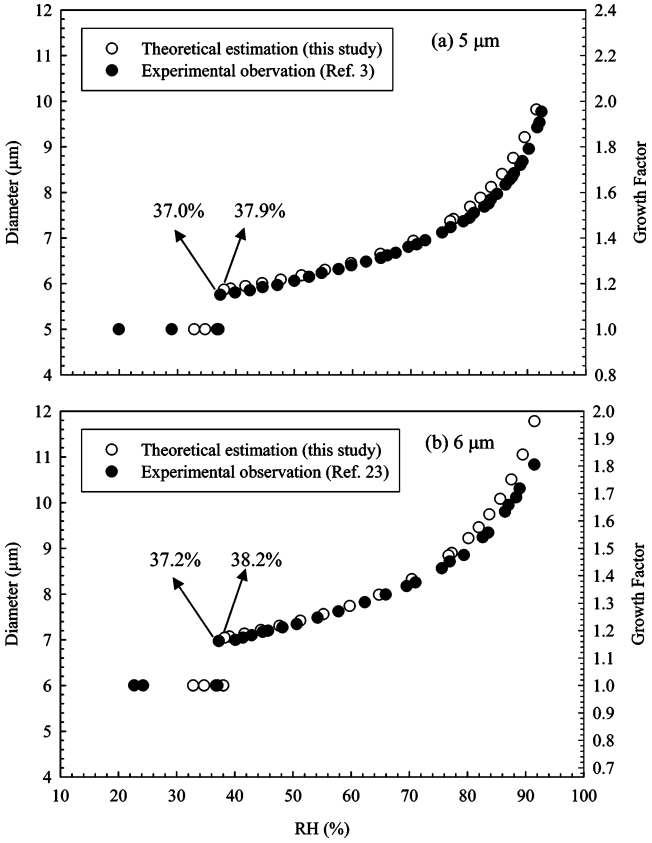

Figure 6. Growth factor and efflorescence trends for AS particles with dry-state diameters of (a) 5 μm and (b) 6 μm.

impurity, which initiates heterogeneous nucleation at a higher ERH.[11,14,22] To verify our suspicion on the data inaccuracy, we use the ERH (38%) for 30 nm AS particles reported by Orr et al.[32] to calculate the corresponding induction time. We find it to be at least 5 h, which is beyond the residence (exposure) time accommodated by their real experimental setup. In addition, the apparatus established by Orr et al.[32] may provide limited accuracy, since the DRH of the AS particles, 75%, reported in the same study also deviates from the consistently observed value, 80%. Taken together, the theoretical prediction appears to provide more reliable estimation for the ERH of 30−80 nm AS particles.

Table 4 lists the predicted ERH of AS dry particles ranging from 8 nm to 30 μm at the fixed induction time of 1 s; the ERH appears to first decrease with the decreasing dry particle size, but become increasing when the dry particles are smaller than 30 nm. This is mainly attributed to the Kelvin effect, which tends to raise the RH (see eq 3) and facilitates a more rapid efflorescence, in particular, for smaller nanometer-sized dry particles. Hence, the theoretical prediction indicates that the Kelvin effect plays an important role in affecting the ERH of AS particles smaller than 30 nm, whereas the aerosol size is the most dominant factor influencing the ERH of particles larger than 50 nm. A similar behavior has recently been observed experimentally for sodium chloride particles by Biskos et al.[20] While the Kelvin effect is expected to be negligible for particles larger than 100 nm,[6,12] this effect on the ERH of nanometer-sized AS particles is, for the first time, elucidated on the basis of classical homogeneous nucleation theory with consistent experimental observation.

TABLE 5: Effect of Induction Time on the Estimated ERH of AS Particle with a Dry Diameter of 100 nm

t (s)	0.01	0.1	0.2	0.5	1	50	100	500	2000	5000
ERH (%)	26.6	28.9	29.6	30.4	31.0	34.1	34.6	35.8	36.6	37.2

Although satisfactory theoretical and experimental observations are provided in this study, it is worthwhile to discuss the difference between experimental and calculated ERHs, which can be attributed to the inaccuracy in the experimentally measured dry particle diameter and in the induction time. The former can be easily understood because our calculation requires a specified dry particle diameter. The latter affects the determination of the critical nucleation rate, according to eq 11, and consequently alters the predicted ERH. With a precise dry particle size of 100 nm, Table 5 shows that the calculated ERH increases with the induction time. However, the calculated ERHs corresponding to various induction times ranging from 0.01 to 2000 s differ from that for 1 s by less than 5.6% RH, which is indeed comparable to the experimental error in this study. To experimentally verify such a modest variation of ERH over a wide range of induction times, one would need an advanced setup, which is capable of accurately measuring RH and also detecting the change of 0.8% RH within 0.1 s for a small induction time (Table 5). Since the actual induction time has not been experimentally measurable using setups similar to what is employed in this study, the residence time is used instead for some cases as an estimate, which should be taken as the upper limit. Hence, our predicted ERH could be higher than the real value.

5. Conclusions

Our theoretically calculated ERHs of suspended ammonium sulfate particles with sizes spanning from 8 nm to 17 μm agree well with experimental data. The ERH appears to first decrease from around 41% when the dry particle size decreases from 30 μm, then increase for the dry particles smaller than 30 nm. The theoretical calculation elucidates that the Kelvin effect plays an important role in affecting the ERH of AS particles smaller than 30 nm, while the aerosol size is the most dominant factor influencing the ERH of particles larger than 50 nm. The theoretical prediction also demonstrates that, to successfully observe ERH of suspended AS particles, the experimental setup needs to provide an RH lower than 29%. The dry particle size and the induction time during homogeneous nucleation are the two major factors affecting the accuracy of theoretically predicted ERH. According to the induction time adopted in this study, the estimated ERH could be somewhat higher than the actual value.

Acknowledgment. The authors are grateful to the financial support from National University of Singapore through grants R-279-000-172-112 and R-279-000-144-112.

References and Notes

(1) Seinfeld, J. H.; Pandis, S. N. *Atmospheric Chemistry and Physics: From Air Pollution to Climate Change*; John Wiley: New York, 1998; pp 507−751.

(2) Berg, O. H.; Swietlicki, E.; Krejci, R. *J. Geophys. Res.* **1998**, *103*, 16535−16545.
(3) Xu, J.; Imre, D.; McGraw, R.; Tang, I. *J. Phys. Chem. B* **1998**, *102*, 7462−7469.
(4) Colberg, C. A.; Krieger, U. K.; Peter, T. *J. Phys. Chem. A* **2004**, *108*, 2700−2709.
(5) Friedbacher, G.; Grasserbauer, M.; Meslmani, Y.; Klaus, N.; Higatsberger, M. J. *Anal. Chem.* **1995**, *67*, 1749−1754.
(6) Hämeri, K.; Vakeva, M.; Hansson H. C.; Laaksonen, A. *J. Geophys. Res.* **2000**, *105*, 22231−22242.
(7) Pant, A.; Fok, A.; Parsons, M. T.; Mak, J.; Bertram, A. K. *Geophys. Res. Lett.* **2004**, *31*, L12111 (1−4).
(8) Cruz, C. N.; Pandis, S. N. *Environ. Sci., & Technol.* **2000**, *34*, 4313−4319.
(9) Schlenker, J. C.; Malinowski, A.; Martin, S. T.; Hung, H. M.; Rudich, Y. *J. Phys. Chem.* **2004**, *108*, 9375−9383.
(10) Cziczo, D. J.; Nowak, J. B.; Hu, J. H.; Abbatt, J. P. D. *J. Geophys. Res.* **1997**, *102*, 18843−18850.
(11) Han, J. H.; Martin, S. T. *J. Geophys. Res.* **1999**, *104*, 3543−2552.
(12) Cohen, M. D.; Flagan, R. C.; Seinfeld, J. H. *J. Phys. Chem.* **1987**, *91*, 4563−4574.
(13) Söhnel, O.; Garside, J. *Precipitation-Basic Principles and Industrial Applications*; Butterworth-Heinemann: Oxford, 1992; pp 42−43.
(14) Onasch, T. B.; McGraw, R.; Imre, D. *J. Phys. Chem. A* **2000**, *104*, 10797−10806.
(15) Clegg, S. L.; Brimblecombe, P.; Wexler, A. S. *J. Phys. Chem. A* **1998**, *102*, 2137−2154.
(16) Clegg, S. L.; Brimblecombe, P.; Wexler, A. S. *J. Phys. Chem. A* **1998**, *102*, 2155−2171.
(17) Mirabel, P.; Reiss, H.; Bowles, R. K. *J. Chem. Phys.* **2000**, *113*, 8200−8205.
(18) Russell, L. M.; Ming, Y. *J. Chem. Phys.* **2002**, *116*, 311−321.
(19) Djikaev, Y. S.; Bowles, R.; Reiss, H.; Hämeri, K.; Laaksonen, A.; Vakeva, M. *J. Phys. Chem. B* **2001**, *105*, 7708−7722.
(20) Biskos, G.; Malinowski, A.; Russell, L. M.; Buseck, P. R.; Martin, S. T. *Aerosol Sci. Technol*. **2006**, *40*, 97−106.
(21) Richardson, C. B.; Snyder, T. D. *Langmuir* **1994**, *10*, 2462−2465.
(22) Lightstone, J. M.; Onasch, T. B.; Imre, D. *J. Phys. Chem. A* **2000**, *104*, 9337−9346.
(23) Tang, I. N.; Munkelwitz, H. R. *J. Geophys. Res.* **1994**, *99*, 18801−18808.
(24) Korhonen, P.; Laaksonen, A.; Batris, E.; Viisanen, Y. *J. Aerosol Sci.* **1998**, *29*, Suppl. 1, S379−S380.
(25) Swietlicki, E.; Zhou, J.; Berg, O. H.; Martinsson, B. G.; Frank, G.; Cederfelt, S. I.; Dusek, U.; Berner, A.; Birmili, W.; Wiedensohler, A.; Yuskiewicz, B.; Bower, K. N. *Atmos. Res.* **1999**, *50*, 205−240.
(26) Chan, C. K.; Flagan, R. C.; Seinfeld, J. H. *Atmos. Environ., A* **1992**, *26*, 1661−1673.
(27) Clegg, S. L.; Ho, S. S.; Chan, C. K.; Brimblecombe, P. *J. Chem. Eng. Data* **1995**, *40*, 1079−1090.
(28) Abraham, M.; Abraham, M. C. *Electrochim. Acta* **2000**, *46*, 137−142.
(29) Ally, M. R.; Clegg, S. L.; Braunstein, J.; Simonson, J. M. *J. Chem. Thermodyn.* **2001**, *33*, 905−915.
(30) Onasch, T. B.; Siefert, R. L.; Brooks, S. D.; Prenni, A. J.; Murray, B.; Wilson, M. A.; Tolbert, M. A. *J. Geophys. Res.* **1999**, *104*, 21317−21326.
(31) Myerson, A. S.; Izmailov, A. F.; Na, H. S. *J. Cryst. Growth* **1996**, *166*, 981−988.
(32) Orr, C., Jr.; Hurd, F. K.; Corbett, W. J. *J. Colloid Sci.* **1958**, *13*, 472−482.